

**This is a self-archived version of an original article. This version may differ from the original in pagination and typographic details.**

**Author(s):** Wang, Yufan; Hietaniemi, Marianna; Välikangas, Juho; Hu, Tao; Tynjälä, Pekka; Lassi, Ulla

**Title:** Effects of Lithium Source and Content on the Properties of Li-Rich Layered Oxide Cathode Materials

**Year:** 2023

**Version:** Published version

**Copyright:** © 2023 by the authors. Licensee MDPI, Basel, Switzerland.

**Rights:** In Copyright




**Rights url:** <http://rightsstatements.org/page/InC/1.0/?language=en>

**Please cite the original version:**

Wang, Y., Hietaniemi, M., Välikangas, J., Hu, T., Tynjälä, P., & Lassi, U. (2023). Effects of Lithium Source and Content on the Properties of Li-Rich Layered Oxide Cathode Materials. *ChemEngineering*, 7(1), Article 15. <https://doi.org/10.3390/chemengineering7010015>

## Article

# Effects of Lithium Source and Content on the Properties of Li-Rich Layered Oxide Cathode Materials

Yufan Wang<sup>1</sup>, Marianna Hietaniemi<sup>1</sup>, Juho Välikangas<sup>1,2</sup>, Tao Hu<sup>1</sup>, Pekka Tynjälä<sup>1,2</sup> and Ulla Lassi<sup>1,2,\*</sup><sup>1</sup> Research Unit of Sustainable Chemistry, University of Oulu, 90014 Oulu, Finland<sup>2</sup> Kokkola University Consortium Chydenius, University of Jyväskylä, 67100 Kokkola, Finland

\* Correspondence: ulla.lassi@oulu.fi; Tel.: +358-400294090

**Abstract:** Lithium-rich layered oxide (LLO) are considered high-capacity cathode materials for next-generation lithium-ion batteries. In this study, LLO cathode materials were synthesized via the hydroxide coprecipitation method followed by a two-step lithiation process using different lithium contents and lithium sources. The effects of lithium content and lithium source on structure and electrochemical performance were investigated. This study demonstrated the clear impact of Li/TM ratio on electrochemical performance. Lower Li/TM ratio reduced the irreversible capacity loss in the first cycle and provided better cycling stability among all samples. The best results exhibited an initial discharge capacity of 279.65 mAh g<sup>-1</sup> and reached a discharge capacity of 231.9 mAh g<sup>-1</sup> (82.9% capacity retention) after 30 cycles. The sample using Li<sub>2</sub>CO<sub>3</sub> as lithium source exhibits better electrochemical performance than the sample using LiOH as lithium source. Therefore, it is important to choose the appropriate lithium source and optimal lithium content for improving structural properties and electrochemical performance of LLO.

**Keywords:** lithium-ion battery; cathode material; lithium-rich layered oxides; coprecipitation; lithium content; lithium source



**Citation:** Wang, Y.; Hietaniemi, M.; Välikangas, J.; Hu, T.; Tynjälä, P.; Lassi, U. Effects of Lithium Source and Content on the Properties of Li-Rich Layered Oxide Cathode Materials. *ChemEngineering* **2023**, *7*, 15. <https://doi.org/10.3390/chemengineering7010015>

Academic Editor: Alirio E. Rodrigues

Received: 1 November 2022

Revised: 31 December 2022

Accepted: 30 January 2023

Published: 14 February 2023



**Copyright:** © 2023 by the authors. Licensee MDPI, Basel, Switzerland. This article is an open access article distributed under the terms and conditions of the Creative Commons Attribution (CC BY) license (<https://creativecommons.org/licenses/by/4.0/>).

## 1. Introduction

Nowadays, exhaustion of fossil fuel, climate change, and environmental pollution are global challenges facing mankind. Sustainable and affordable energies have attracted much attention in the past decades [1,2]. Rechargeable lithium-ion batteries (LIBs) are considered to be the key technology to reduce carbon dioxide emissions from transportation, power, and industry sectors, and to enable low-carbon or zero-carbon society [3,4]. However, the energy density of commercialized cathode materials still limits large-scale application of electric vehicles and grid-scale energy storage. To meet the demands, advanced LIBs with high energy density, long cycle life, good thermal stability, low-cost and environmental compatibility are needed [5–7]. Lithium-rich layered oxide (LLO) are considered one of the most promising cathode materials for next-generation LIBs [3,8,9]. LLO cathode materials can deliver a specific capacity of over 250 mAh g<sup>-1</sup> and an energy density of approximately 1000 Wh kg<sup>-1</sup> at room temperature [4,5,10]. Currently, commercialized cathode materials have layered LiCoO<sub>2</sub>, spinel LiMn<sub>2</sub>O<sub>4</sub>, olivine LiFePO<sub>4</sub>, and layered mixed transition-metal oxides LiNi<sub>x</sub>Co<sub>y</sub>Mn<sub>1-x-y</sub>O<sub>2</sub> and LiNi<sub>1-x-y</sub>Co<sub>x</sub>Al<sub>y</sub>O<sub>2</sub> [6,10]. These conventional cathode materials are limited to their practical capacities of around 120–200 mAh g<sup>-1</sup> [4,5,10]. Compared with these common cathode materials, LLO has the advantages of high discharge capacity, a wide operating voltage plateau, cost-effectiveness, and environmental friendliness [7,11].

The history of the development of LLO cathode materials goes back to the 1990s. Thackeray et al. [12] demonstrated that lithium manganese oxide Li<sub>2-x</sub>MnO<sub>3-x/2</sub> serves as cathode material in LIBs. The electrochemically active Li<sub>1.09</sub>Mn<sub>0.91</sub>O<sub>2</sub> was synthesized via chemical leaching of Li<sub>2</sub>O from Li<sub>2</sub>MnO<sub>3</sub> under the acid treatment method. In 1997, Numata et al. [13,14] identified a layered solid solution of the LiCoO<sub>2</sub>-Li<sub>2</sub>MnO<sub>3</sub> system as

cathode material. In 1999, Kalyani et al. [15] first demonstrated that  $\text{Li}_2\text{MnO}_3$  could be electrochemically activated at a voltage of approximately 4.5 V without acid treatment. In 2001, Lu et al. [16] synthesized layered  $\text{Li}[\text{Ni}_x\text{Li}_{(1/3-2x/3)}\text{Mn}_{(2/3-x/3)}]\text{O}_2$  using the hydroxide coprecipitation method, which provided a discharge capacity of about  $200 \text{ mAh g}^{-1}$  in the range of 2.0–4.6 V. From 2001 to 2004, many studies reported that LLO cathode materials provided a high discharge capacity over  $200 \text{ mAh g}^{-1}$  in the range of 2.0–4.8 V [7,10,17,18]. In 2005, Thackeray et al. [8] introduced the concept of Li- and Mn-rich layered oxides as high-capacity cathode materials for next-generation LIBs. Since that time, LLO cathode materials have attracted much attention; many studies have focused on revealing their crystal structure and reaction mechanisms and developed modification strategies for improving electrochemical performance [8,19–23].

Generally, LLO cathode materials can be presented as  $x\text{Li}_2\text{MnO}_3 \cdot \cdot (1-x)\text{LiMO}_2$  or  $\text{Li}_{1+x}\text{M}_{1-x}\text{O}_2$ , where M is transition metals,  $0 < x < 1$  [5,8,24]. The studied M includes single transition metals or a combination of several transition metals, such as Mn, Co, Cr, Ti, Zr, Mn-Cr, Mn-Fe, Mn-Co, Ni-Mn, Ni-Co-Mn, etc. [9,13,14,16–18]. The common LLO cathode materials have Ni-Mn oxides, such as  $\text{Li}_{1.2}\text{Ni}_{0.2}\text{Mn}_{0.6}\text{O}_2$ , and Ni-Mn-Co oxides, such as  $\text{Li}_{1.2}\text{Mn}_{0.54}\text{Ni}_{0.13}\text{Co}_{0.13}\text{O}_2$  [6,10]. LLO cathode materials consist of a monoclinic layered  $\text{Li}_2\text{MnO}_3$  phase with the space group  $\text{C2/m}$  and a trigonal layered  $\text{LiMO}_2$  phase with the space group  $\text{R}\bar{3}\text{m}$  [10,22]. The synergistic effects of  $\text{Li}_2\text{MnO}_3$  and  $\text{LiMO}_2$  deliver a high discharge capacity over  $250 \text{ mAh g}^{-1}$  within a wide voltage range of 2.0–4.8 V [6,10]. The high-capacity LLO cathode materials result from TM ion redox reactions and oxygen anion redox reactions [11]. Lithium ions are extracted from  $\text{LiMO}_2$  accompanied by the oxidation of  $\text{Ni}^{2+}/\text{Ni}^{3+}$  to  $\text{Ni}^{4+}$  and  $\text{Co}^{3+}$  to  $\text{Co}^{4+}$  in the range of 2.0–4.4 V [10,25]. In this region,  $\text{Li}_2\text{MnO}_3$  can stabilize the structure but does not contribute to capacities [26]. The  $\text{Li}_2\text{MnO}_3$  component will be activated in the range of 4.4–4.8 V, leading to irreversible removal of  $\text{Li}^+$  and  $\text{O}^{2-}$  to form  $\text{Li}_2\text{O}$  and electrochemically active  $\text{MnO}_2$  [8]. Therefore, LLO cathode materials suffer from a high irreversible capacity loss of 40–100  $\text{mAh g}^{-1}$  and a low Coulombic efficiency of approximately 80% during the initial charge–discharge cycle [6,10]. Moreover, LLO cathode materials have the drawbacks of voltage and capacity fading due to irreversible layered-to-spinel structural changes and undesirable side reactions on the electrode interface [5,7,10]. The poor rate capability of LLO cathode materials is related to the low kinetic diffusion of  $\text{Li}^+$  ions and the low electronic conductivity of  $\text{Li}_2\text{MnO}_3$  [7,10]. To overcome these challenges and improve electrochemical performance, various modification strategies have been employed, such as chemical activation, optimizing the synthesis method, surface coating, ion doping, and the use of nanosized materials [7,10,27,28]. It is also necessary to better understand the properties and electrochemical performance of LLO cathode materials.

In this study, LLO cathode materials were synthesized using the hydroxide coprecipitation method followed by a two-step lithiation process. The impacts of different lithium contents and lithium sources on structure and electrochemical performance were examined. This study provides a new understanding of the relationship between synthesis conditions and the electrochemical performance of LLO cathode materials.

## 2. Materials and Methods

### 2.1. Material Synthesis

As Figure 1 shows, the LLO cathode materials were synthesized using a two-step process: (i) the synthesis of  $\text{Mn}_{0.675}\text{Ni}_{0.1625}\text{Co}_{0.1625}(\text{OH})_2$  precursors via coprecipitation and (ii) the blending of the precursors with lithium sources ( $\text{LiOH}$  or  $\text{Li}_2\text{CO}_3$ ) to synthesize final products via calcination at high temperature [29,30].

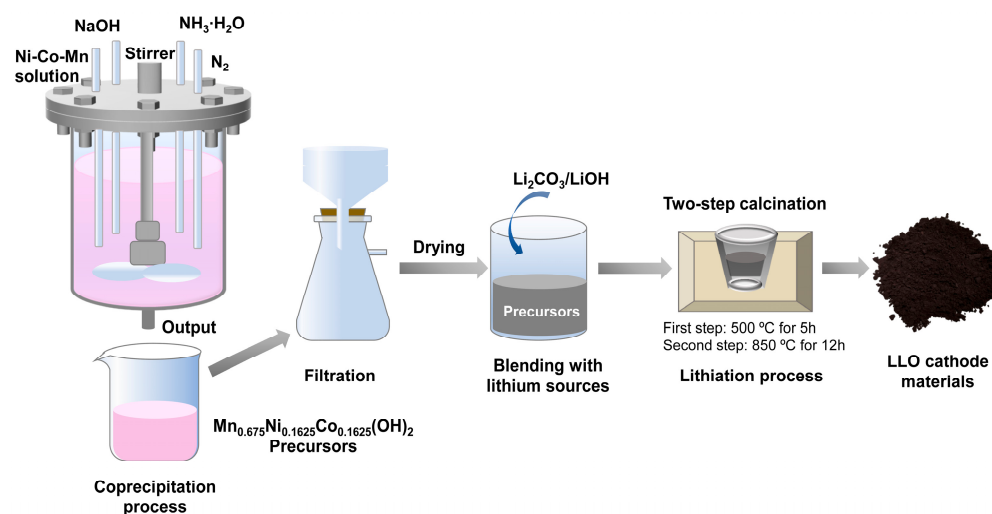


**Figure 1.** Schematic diagram of the synthesis of LLO cathode materials.

The synthesis of  $\text{Mn}_{0.675}\text{Ni}_{0.1625}\text{Co}_{0.1625}(\text{OH})_2$  precursors was conducted in a batch process. Distilled water (800 mL) containing a concentration of 10 g/L  $\text{NH}_3 \cdot \text{H}_2\text{O}$  as the starting solution was fed into a continuous stirred-tank reactor with a capacity of 4 L. Stoichiometric amounts of  $\text{MnSO}_4 \cdot \text{H}_2\text{O}$ ,  $\text{NiSO}_4 \cdot 6\text{H}_2\text{O}$ , and  $\text{CoSO}_4 \cdot 7\text{H}_2\text{O}$  (molar ratio of  $\text{Mn}/\text{Ni}/\text{Co} = 0.675:0.1625:0.1625$ ) were dissolved in distilled water to prepare a 2M TM solution. Then, the 2M TM solution, with a feed rate of 4 mL/min, and 2M NaOH as a precipitant, with a feed rate of 7.4 mL/min, were continuously pumped into the reactor. Simultaneously, 2M  $\text{NH}_3 \cdot \text{H}_2\text{O}$  as a chelating agent was pumped into the reactor at a feed rate of 1.2 mL/min. The pH was controlled with the addition of 2M NaOH to maintain the pH of the solution system at 11.5. The process was conducted at 55 °C and with a stirring speed of 800 rpm for 4 h under an  $\text{N}_2$  atmosphere. After the coprecipitation process, the mixture solution was filtered, washed with distilled water a few times, and dried in a vacuum at 60 °C overnight under  $\text{N}_2$ . Then, the obtained hydroxide precursors were blended with a stoichiometric amount of the lithium source,  $\text{Li}_2\text{CO}_3$  or LiOH. The final products were obtained by preheating at 500 °C for 5 h and then by calcination at 850 °C for 12 h with a heating rate of 5 °C  $\text{min}^{-1}$  under an air atmosphere. A 10 wt% excess of  $\text{Li}_2\text{CO}_3$  or LiOH was added to compensate for lithium loss during the lithiation process.

## 2.2. Material Characterization

The particle size distributions were analyzed using a Mastersizer 3000 (Malvern Panalytical, Almelo, The Netherlands) particle analyzer with an attached Hydro EV sample 100 dispersion unit. The refractive-index and absorption-index values were 1.7 and 0.006 for the precursors and 3.0 and 0.02 for the LLO cathode materials, respectively. The tapped density of the precursors and LLO cathode materials was measured using an Erweka SVM222 tapped density device following the ISO EN 787/11 standard. The chemical composition of Li, Ni, Mn, and Co in the synthesized materials was measured via inductively coupled plasma-optical emission spectroscopy (ICP-OES; Agilent 5110 VDV). ICP-OES analysis was performed on solid precipitates, and the corresponding Li:Ni:Co:Mn ratio was confirmed. Microwave digestion was used to dissolve these samples completely without any leaching residue. This was performed using nitric acid based on the EPA3051A standard: hydrochloric acid as a solvent with a ratio of 3:1. The morphology of the cathode materials was characterized using Zeiss Sigma field emission scanning electron microscopy (Carl Zeiss Microscopy GmbH, Jena, Germany) at the Centre for Material Analysis, University of Oulu. X-ray diffraction (XRD) patterns were recorded with a PANalytical X'Pert Pro XRD diffractometer (Malvern Panalytical, Almelo, The Netherlands) using monochromatic  $\text{CuK}\alpha 1$  radiation ( $\lambda = 1.5406 \text{ \AA}$ ) at 45 kV and 40 mA. Diffractograms were collected in the  $2\theta$  range of 15–90° at 0.017° intervals. The crystalline phases and



structures were analyzed using HighScore Plus software version 4.0 (PANalytical B. V., Almelo, The Netherlands) using the Rietveld analysis method.

### 2.3. Electrochemical Measurements

The slurry of cathode materials was prepared by 80 wt% cathode materials, 10 wt% carbon black (Timcal Super C45), and 10 wt% polyvinylidene fluoride (Kureha #1100). The mixture was dissolved in the appropriate amount of N-methyl-2-pyrrolidone (Alfa Aesar, anhydrous 99.5%) and was mixed in a slurry mixer to obtain a uniform slurry. The slurry consisted of approximately 40 wt% solid matter. The uniform slurry was coated on the aluminum foil current collector with 100- $\mu\text{m}$  applicators and dried in a vacuum at 120 °C overnight. The dried cathode material was pressed via calendaring pressing. The coin cells (type 2016) were assembled with cathode material, a lithium metal reference electrode, a separator, and an electrolyte under dry room conditions. The electrolyte consisted of 1 M lithium hexafluorophosphate (LiPF<sub>6</sub>; Novolyte Technologies) dissolved in ethylene carbonate (EC), diethyl carbonate (DEC), and dimethyl carbonate (DMC) (1:1:1 vol% ratio) (EC: Sigma-Aldrich, anhydrous 99%; DEC: Sigma-Aldrich, anhydrous 99%; DMC: Novolyte Technologies, 99% sealed under nitrogen). The active material loading of electrodes was maintained at around 5.0 mg cm<sup>-2</sup>. The electrochemical performance of the assembled coin cells was tested using a Maccor battery tester in constant-current mode at 25 °C. The testing program was performed on the first cycle at 0.03 C and following 30 cycles at 0.1 C in the range of 2.0–4.8 V. The theoretical capacity used to calculate the C-rate was 200 mAh g<sup>-1</sup>.

## 3. Results and Discussion

### 3.1. Effect of Lithium Content on Structure and Electrochemical Performance

Lithium is one of the most essential elements in LLO cathode materials. Lithium content affects the structure and electrochemical performance of LLO cathode materials [5,10,31]. The theoretical lithium content used in the synthesis of typical LLO cathode materials is Li<sub>1.2</sub>Mn<sub>0.54</sub>Ni<sub>0.13</sub>Co<sub>0.13</sub>O<sub>2</sub> with an Li/TM ratio of 1.5:1 [29]. In this study, the LLO cathode materials were synthesized with a variety of Li/TM ratios. Table 1 presents the chemical composition of samples L10–L13. The impacts of various Li/TM ratios on structure and electrochemical performance were investigated.

**Table 1.** Chemical composition of samples L10–L13 prepared by various Li/TM ratios.

Sample	Li	Experimental Li/Mn/Ni/Co Molar Ratio			Li/TM Ratio	Chemical Formula
		Mn	Ni	Co		
L10	1.31	0.57	0.15	0.15	1.52	Li <sub>1.31</sub> Mn <sub>0.57</sub> Ni <sub>0.15</sub> Co <sub>0.15</sub> O <sub>2</sub>
L11	1.31	0.53	0.14	0.14	1.64	Li <sub>1.31</sub> Mn <sub>0.53</sub> Ni <sub>0.14</sub> Co <sub>0.14</sub> O <sub>2</sub>
L12	1.23	0.47	0.12	0.12	1.73	Li <sub>1.23</sub> Mn <sub>0.47</sub> Ni <sub>0.12</sub> Co <sub>0.12</sub> O <sub>2</sub>
L13	0.89	0.32	0.08	0.08	1.86	Li <sub>0.89</sub> Mn <sub>0.32</sub> Ni <sub>0.08</sub> Co <sub>0.08</sub> O <sub>2</sub>

Figure 2a shows the XRD patterns of samples L10–L13. All the major peaks were well indexed to a hexagonal  $\alpha$ -NaFeO<sub>2</sub> layered structure with the R $\bar{3}$ m space group (ICDD file 04-023-1600), except for the small peaks between 20° and 25°, which are characteristic of Li<sub>2</sub>MnO<sub>3</sub> with the C2/m space group (ICDD file 01-082-2663) [19]. In L10–L13, the clear splitting peaks of (006)/(012) and (018)/(110) were sharp and intense, which indicated that well-layered structure materials were successfully synthesized [31]. In addition, the weak peaks between 20° and 25° provided evidence of existing Li<sub>2</sub>MnO<sub>3</sub> phases in the synthesized materials. These characteristic peaks of Li<sub>2</sub>MnO<sub>3</sub> were indexed to a monoclinic structure with the C2/m space group [19,26]. No other impurities or spinel-phase peaks were observed in the prepared materials. The XRD results demonstrated that the prepared samples L10–L13 had good crystallinity, a well-layered structure, and a high-purity phase.

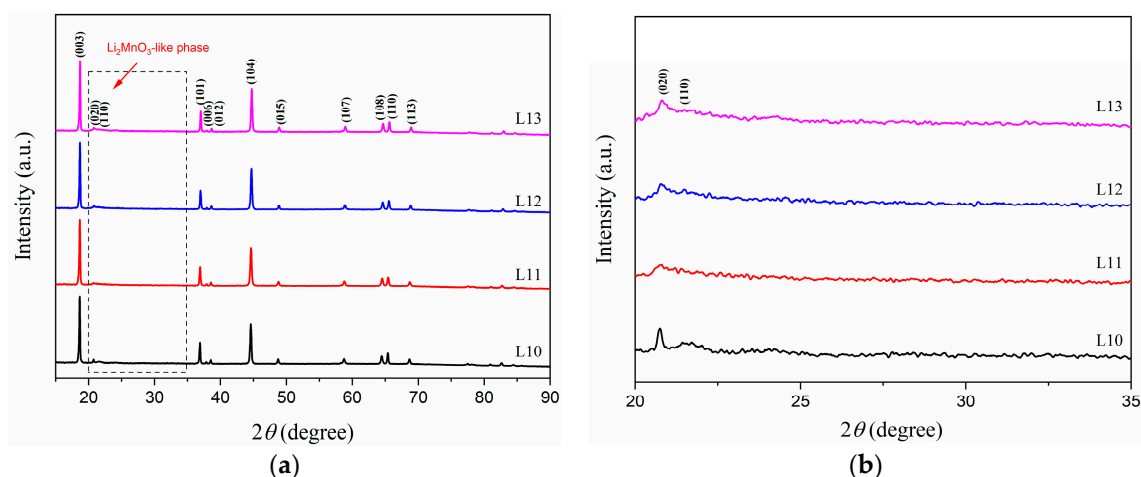


**Figure 2.** (a) XRD patterns of samples L10–L13; (b) Magnified rectangle region in (a): superlattice peaks of C2/m  $\text{Li}_2\text{MnO}_3$  in the  $2\theta$  range of 20–25°.

However, samples L10–L13 exhibited slight differences in peak intensity between 20° and 25°, as Figure 2b shown. The superlattice peaks of (020) and (110) for L10 were sharper and more intense than those of L11, L12, and L13. Broad peaks were observed in L11, L12, and L13, which may have been associated with the presence of less Mn content in the samples, resulting in insufficient Mn to form the  $\text{LiMn}_6$  superstructure in the  $\text{Li}_2\text{MnO}_3$  phase [32]. Moreover, the refined lattice parameters of the monoclinic  $\text{Li}_2\text{MnO}_3$  phase in samples L10–L13 are compared in Table 2. The ideal lattice parameters of monoclinic  $\text{Li}_2\text{MnO}_3$  with the C2/m space group are  $a = 4.937 \text{ \AA}$ ,  $b = 8.532 \text{ \AA}$ ,  $c = 5.030 \text{ \AA}$ ,  $\alpha = \gamma = 90^\circ$ , and  $\beta = 109.46^\circ$  [19]. It can be seen that the values of L10 were the closest to the ideal lattice parameter of  $\text{Li}_2\text{MnO}_3$ , which indicated that L10 had a higher crystallinity than L11, L12, and L13. Different degrees of broadening peaks between 20° and 25° were observed in L10–L13. The existence of defects and stacking faults usually leads to the weakening and broadening of superlattice peaks [33–35]. L11 had weaker peak intensities of (020) and (110), which may have been caused by the smaller  $c$  value of  $5.017 \text{ \AA}$  than that of L10, L12 and L13. It was found that the disordered stacking ordering along the  $c$ -axis may have resulted in weak or broad superlattice peaks, even if the arrangement of  $\text{Li}^+$  and  $\text{Mn}^{4+}$  in TM layers was ordered [33,34]. Furthermore, the stacking faults may have been due to the existence of  $\text{Ni}^{2+}$  and  $\text{Co}^{3+}$  in TM layers [35]. Boulineau et al. [34] suggested that different levels of stacking faults can be roughly estimated by comparing the intensity ratios of (110) and (020) peaks ( $I_{(110)}/I_{(020)}$ ) in  $\text{Li}_2\text{MnO}_3$ . The experimental results indicated that increasing the synthesis temperature during calcination may have decreased the degree of stacking faults but that it could not entirely eliminate them [34].

**Table 2.** Lattice parameters of samples L10–L13 for existence of the monoclinic  $\text{Li}_2\text{MnO}_3$  phase.

Sample	$a/\text{\AA}$	$b/\text{\AA}$	$c/\text{\AA}$	Alpha/ $^\circ$	Gamma/ $^\circ$	Beta/ $^\circ$
L10	4.937	8.534	5.028	90	90	109.64
L11	4.928	8.527	5.017	90	90	109.31
L12	4.916	8.518	5.033	90	90	109.46
L13	4.916	8.511	5.027	90	90	109.41

Figure 3a presents the initial charge–discharge curves of samples L10–L13 at 0.03 C in the range of 2.0–4.8 V. All the samples had charge characteristics typical of LLO cathode materials: the first sloping plateau extended from 3.8 to 4.4 V, and the second plateau was above 4.4 V. The first plateau was associated with the extraction of lithium ions from the  $\text{LiMO}_2$  component corresponding to  $\text{Ni}^{2+}/\text{Ni}^{3+}$  to  $\text{Ni}^{4+}$  and  $\text{Co}^{3+}$  to  $\text{Co}^{4+}$  [10,25]. All the samples delivered a TM redox capacity of approximately  $70\text{--}120 \text{ mAh g}^{-1}$  in the first

plateau. The second plateau region exhibited a long plateau above 4.4 V that provided additional charge capacities due to the extraction of lithium ions accompanied by O<sub>2</sub> loss from the Li<sub>2</sub>MnO<sub>3</sub> component [10,25]. Therefore, a large, irreversible loss of capacities in the initial cycle was observed in the prepared samples, which resulted mainly from the irreversible removal of Li<sub>2</sub>O from the Li<sub>2</sub>MnO<sub>3</sub> component. Inactive Li<sub>2</sub>MnO<sub>3</sub> then became electrochemically active MnO<sub>2</sub> (Li<sub>2</sub>MnO<sub>3</sub> → Li<sub>2</sub>O + MnO<sub>2</sub>). As Table 3 shows, the initial charge/discharge capacities of L10, L11, L12, and L13 were 337.8/279.7 mAh g<sup>-1</sup>, 325.7/255.2 mAh g<sup>-1</sup>, 311.8/241.3 mAh g<sup>-1</sup>, and 348.28/221.44 mAh g<sup>-1</sup>, respectively. L10, L11, and L12 had an irreversible capacity loss of around 20% in the first cycle, whereas L13 had an irreversible capacity loss of approximately 40% in the first cycle. L10 delivered the highest initial Coulombic efficiency (82.8%), with an irreversible capacity loss of 58.12 mAh g<sup>-1</sup>. L13 exhibited the highest initial charge capacity (348.28 mAh g<sup>-1</sup>) but had the lowest initial Coulombic efficiency (63.6%), with an irreversible capacity loss of 126.84 mAh g<sup>-1</sup>. The oxygen-loss plateau above 4.4 V disappeared in the second cycle, which implied an irreversible structural evolution for the synthesized materials, as shown in Figure 3b [8,10,25]. Figure 3c compared the voltage profiles of L10–L13 for the 3rd discharge and 31st discharge. All samples exhibited continuous voltage fading during cycling, whereas L13 display the most obvious voltage drop, shown in Figure 3d. It implied that the structural changes from layered to spinel phases were due to lattice oxygen release and transition metal migration during Li<sub>2</sub>MnO<sub>3</sub> activation process [10,36].

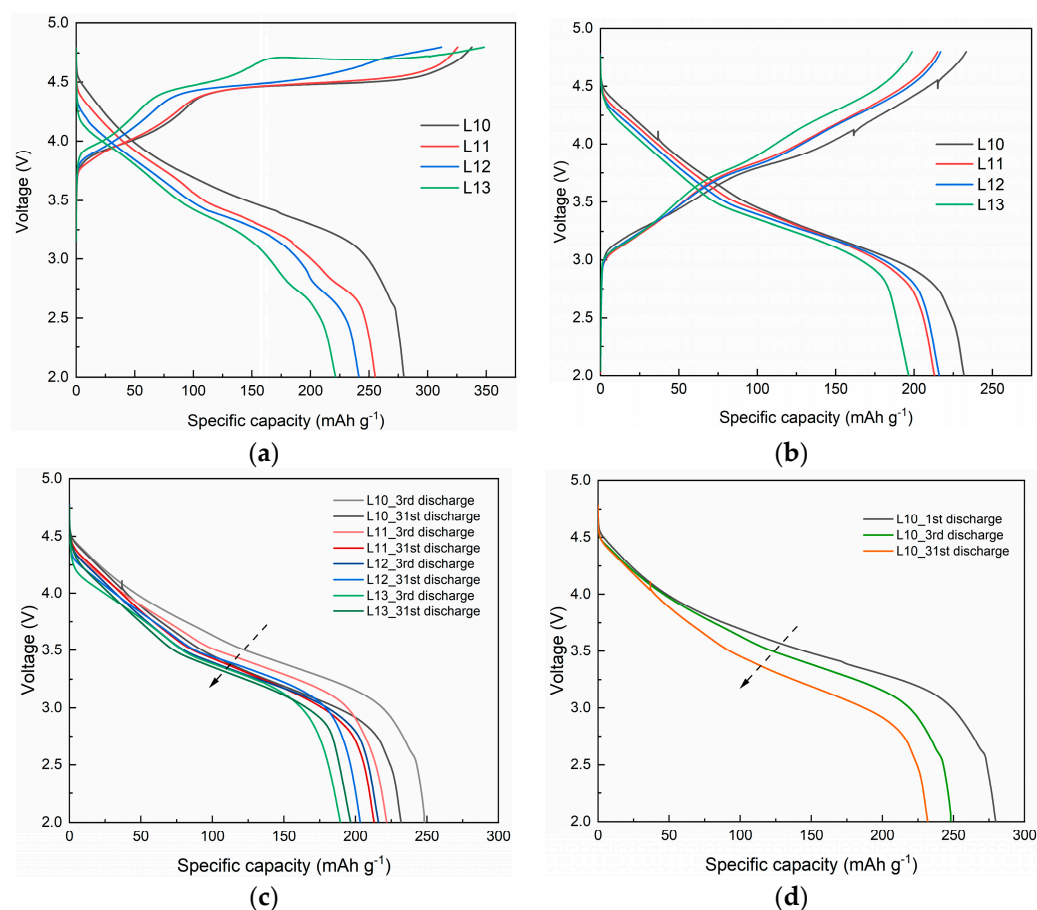


**Figure 3.** (a) Initial charge–discharge profiles of L10–L13 at 0.03 C within 2.0–4.8 V; (b) charge–discharge profiles of L10–L13 for the 31st cycle at 0.1C within 2.0–4.8 V; (c) Voltage profiles of L10–L13 for comparison of 3rd discharge and 31st discharge; (d) Voltage profiles of L10 for comparison of the 1st discharge, 3rd discharge and 31st discharge.

**Table 3.** Initial charge–discharge performance of samples L10–L13 at 0.03 C within 2.0–4.8 V.

Sample	Initial Charge Capacity/mAh g <sup>-1</sup>	Initial Discharge Capacity/mAh g <sup>-1</sup>	Irreversible Capacity/mAh g <sup>-1</sup>	Initial Coulombic Efficiency/%
L10	337.77	279.65	58.12	82.8
L11	325.66	255.23	70.43	78.4
L12	311.75	241.34	70.41	77.4
L13	348.28	221.44	126.84	63.6

Figure 4a shows the cycling performance of samples L10–L13 for 30 cycles in the range of 2.0–4.8 V. During the second cycle, all samples decreased the discharge capacities of 30–40 mAh g<sup>-1</sup> when the current rates changed from 0.03 C to 0.1 C. L10 displayed better cycling performance than L11, L12 and L13. L12 has slightly fluctuated and slowly increased the discharge capacity during cycling. The Li<sub>2</sub>MnO<sub>3</sub> component in L12 may not be entirely activated in the first cycle, which led to the discharge capacity's continuous increase with increasing cycle numbers. In addition, sample L13 had lower discharge capacities than those of L10, L11, and L12 for 30 cycles. This is probably related to the presence of lower lithium and TM content in sample L13, which increased metal vacancies and lithium vacancies in the crystal structure, resulting in L13's decreased structural stability and poor cycling performance [31,37]. Moreover, these results suggested that coin cells could be tested for three cycles under low current density to fully activate Li<sub>2</sub>MnO<sub>3</sub> component. This could help to improve the cycling stability of LLO cathode materials.

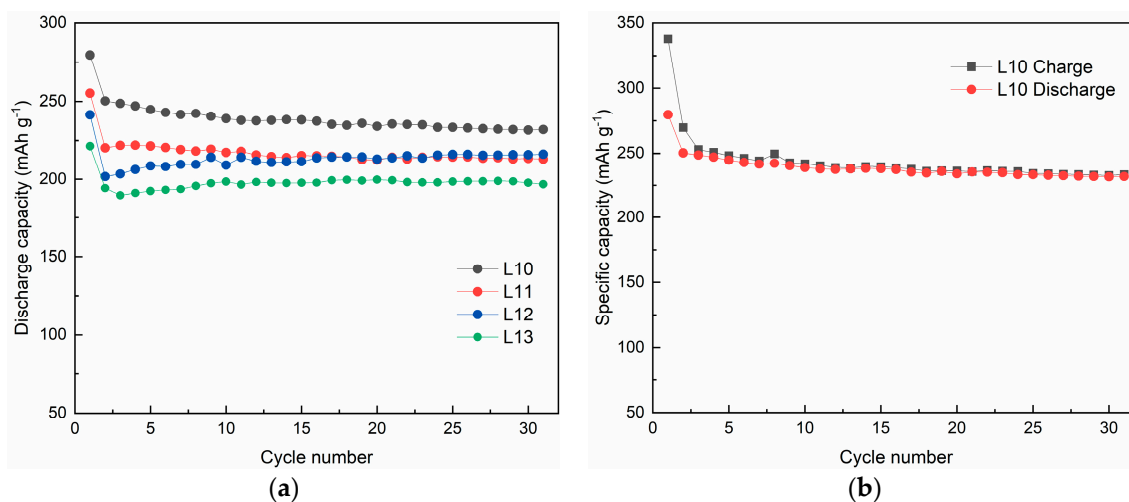


**Figure 4.** (a) Cycling performance of samples L10–L13 for 30 cycles in the range of 2.0–4.8 V; (b) Charge–discharge curves of sample L10 for 30 cycles in the range of 2.0–4.8 V.

After 30 cycles, the discharge capacities of L10, L11, L12, and L13 were 231.9 mAh g<sup>-1</sup>, 213.1 mAh g<sup>-1</sup>, 216.2 mAh g<sup>-1</sup>, and 196.7 mAh g<sup>-1</sup>, respectively. Overall, given L10's low Li/TM ratio, it exhibited the highest discharge capacity, lowest initial irreversible capacity loss, and good cycling stability among the four samples, as Figure 4b shown. This was in good agreement with the XRD results for L10, which indicated a good crystalline structure and fewer defects in the Li<sub>2</sub>MnO<sub>3</sub> structure. With increasing lithium content and TM content, the discharge capacities and cycling stability of samples L10–L13 increased. As the lithium content and TM content decreased in L13, the charge and discharge capacities decreased, and more vacancies were generated in the structure of the material. These vacancies may have increased the diffusion rate of lithium ions and led to an unstable structure and reduced cycling stability [31]. The results suggested that lithium content can optimize electrochemical performance by adjusting the proportion of Li<sub>2</sub>MnO<sub>3</sub> in LLO cathode materials [10,31]. For example, Shunmugasundaram et al. [38] confirmed that a lower Li/TM ratio could reduce irreversible capacity loss in the first cycle. A suitable

$\text{Li}_2\text{MnO}_3$  proportion can stabilize the crystal structure and cycling performance. In addition, excessive lithium content causes a large initial irreversible capacity loss, increased residual lithium on the surface, and deterioration of electrochemical performance [10,31].

### 3.2. Effect of Lithium Sources on Structure and Electrochemical Performance

Different lithium sources exert different effects on the structure and electrochemical properties of LLO cathode materials.  $\text{Li}_2\text{CO}_3$  and  $\text{LiOH}$ , the most common lithium sources, are used in cathode material for LIBs [30]. The effects of lithium sources on structure and electrochemical performance were investigated. The LLO cathode materials L12 and L15 were prepared using different lithium sources ( $\text{Li}_2\text{CO}_3$  and  $\text{LiOH}$ , respectively). Table 4 presents the chemical composition of L12 and L15.

**Table 4.** Chemical composition of samples L12 and L15 prepared by different lithium sources.

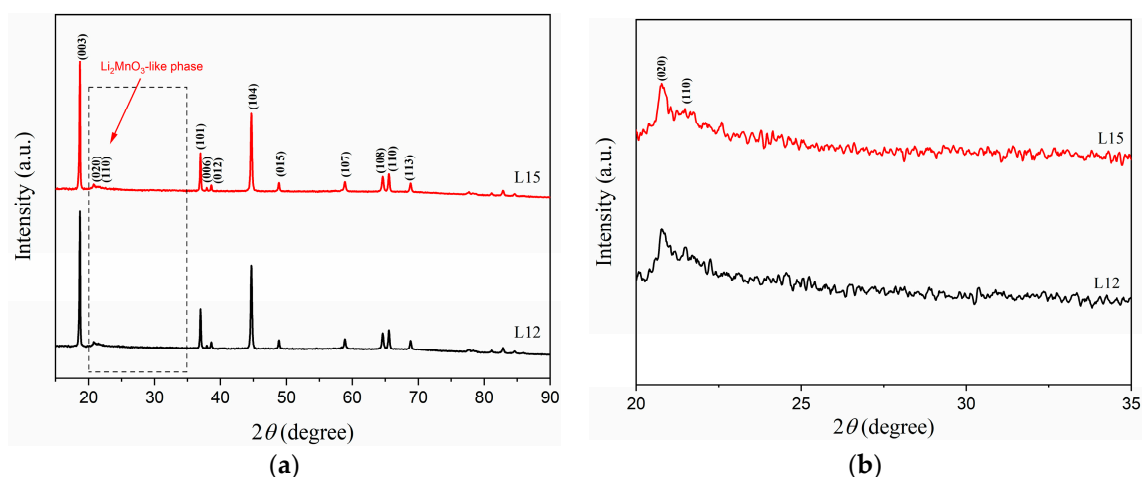
Sample	Lithium Source	Experimental Li/Mn/Ni/Co Molar Ratio				Chemical Formula
		Li	Mn	Ni	Co	
L12	$\text{Li}_2\text{CO}_3$	1.23	0.47	0.12	0.12	$\text{Li}_{1.23}\text{Mn}_{0.47}\text{Ni}_{0.12}\text{Co}_{0.12}\text{O}_2$
L15	$\text{LiOH}$	1.24	0.49	0.12	0.12	$\text{Li}_{1.24}\text{Mn}_{0.49}\text{Ni}_{0.12}\text{Co}_{0.12}\text{O}_2$

Figure 5a shows the XRD patterns of L12 (using  $\text{Li}_2\text{CO}_3$  as a lithium source) and L15 (using  $\text{LiOH}$  as a lithium source). For samples L12 and L15, all the major peaks could be indexed to a hexagonal  $\alpha\text{-NaFeO}_2$  layered structure with the  $R\bar{3}m$  space group (ICDD file 04-023-1600) [19]. Superlattice peaks between  $20^\circ$  and  $25^\circ$  were observed in the two samples, which could be indexed to monoclinic  $\text{Li}_2\text{MnO}_3$  with the  $C2/m$  space group (ICDD file 01-082-2663) [19,26]. The materials synthesized by  $\text{Li}_2\text{CO}_3$  and  $\text{LiOH}$  had a similar peak intensity of (020) and (110), as Figure 5b shows. The refined lattice parameter of the  $\text{Li}_2\text{MnO}_3$  phase in these two samples is described in Table 5. L12 and L15 had a crystallinity similar to that of the  $\text{Li}_2\text{MnO}_3$  phase. The two samples exhibited certain defects in the crystal structure of the  $\text{Li}_2\text{MnO}_3$  phase compared to the ideal lattice parameters of monoclinic  $\text{Li}_2\text{MnO}_3$ . The lattice parameters of monoclinic  $\text{Li}_2\text{MnO}_3$  are  $a = 4.937 \text{ \AA}$ ,  $b = 8.532 \text{ \AA}$ ,  $c = 5.030 \text{ \AA}$ ,  $\alpha = \gamma = 90^\circ$ , and  $\beta = 109.46^\circ$  [19]. Clear splitting peaks, of (006)/(012) and (018)/(110), and no impurity peaks were observed. The XRD results indicated that the two samples synthesized by  $\text{Li}_2\text{CO}_3$  and  $\text{LiOH}$  had good crystallinity, a well-layered structure, and a high-purity phase [30,31]. In addition, the SEM images of L12 and L15 are compared in Figure 6. Both samples exhibited irregular morphology and small, round-edged primary particles, which contained a substantial agglomeration of particles. The morphology of the two samples was unaffected by the lithium source with which they were prepared.

**Table 5.** Lattice parameters of samples L12 and L15 for existence of the monoclinic  $\text{Li}_2\text{MnO}_3$  phase.

Sample	Lithium Source	a/Å	b/Å	c/Å	Alpha/°	Gamma/°	Beta/°
L12	$\text{Li}_2\text{CO}_3$	4.916	8.518	5.033	90	90	109.46
L15	$\text{LiOH}$	4.920	8.516	5.035	90	90	109.41





**Figure 5.** (a) XRD pattern of synthesized material with different lithium sources: LiOH and Li<sub>2</sub>CO<sub>3</sub>; (b) Magnified rectangle region in (a): superlattice peaks of C2/m Li<sub>2</sub>MnO<sub>3</sub> in the 2θ range of 20–25°.

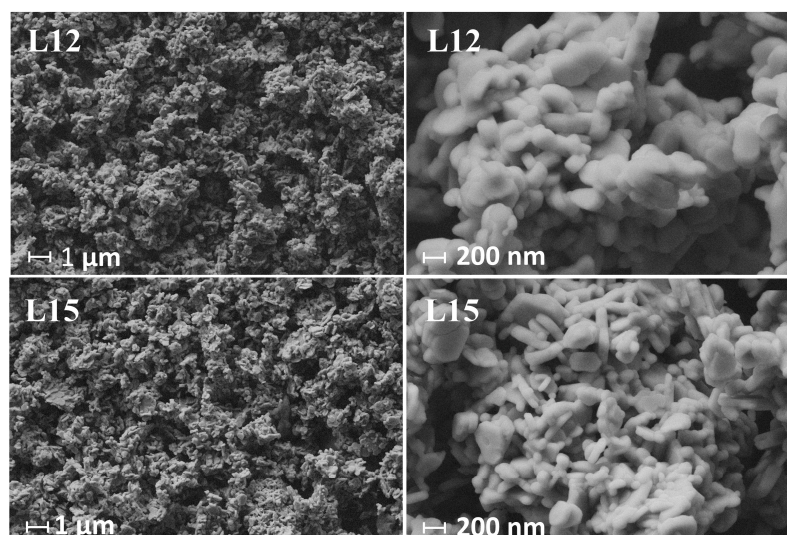


**Figure 6.** SEM images of samples L12 and L15 under different degrees of magnification.

Figure 7a shows the initial charge–discharge curves of L12 and L15, prepared using the lithium sources of Li<sub>2</sub>CO<sub>3</sub> and LiOH, respectively, in the range of 2.0–4.8 V. The two typical plateaus of LLO cathode material were observed in the initial charging curves for L12 and L15. During the initial charging process, the first plateau, from 3.8 to 4.4 V, was related to the reversible extraction of Li<sup>+</sup> from the LiMO<sub>2</sub> component corresponding to the oxidation of Ni<sup>2+</sup>/Ni<sup>3+</sup> to Ni<sup>4+</sup> and Co<sup>3+</sup> to Co<sup>4+</sup> [10,25]. At the first plateau, L12 and L15 had a similar TM redox capacity of around 90 mAh g<sup>−1</sup>. The second long plateau, above 4.4 V, corresponded to the irreversible extraction of Li<sup>+</sup> and O<sup>2−</sup> as Li<sub>2</sub>O from the Li<sub>2</sub>MnO<sub>3</sub> component. The electrochemically active MnO<sub>2</sub> was formed and the long plateau disappeared after the first cycle, which implied irreversible changes of structure for the synthesized materials [8,30]. In the range of 2.0–4.8 V, the initial charge and discharge capacities of L12, prepared using Li<sub>2</sub>CO<sub>3</sub> as a lithium source, were 311.8 mAh g<sup>−1</sup> and 241.3 mAh g<sup>−1</sup>, respectively. L15, prepared using LiOH as a lithium source, exhibited an initial charge capacity of 311.7 mAh g<sup>−1</sup> and an initial discharge capacity of 230.9 mAh g<sup>−1</sup>. As Table 6 shows, the irreversible capacity losses of L12 and L15 were 70.4 mAh g<sup>−1</sup> and 80.8 mAh g<sup>−1</sup>, respectively. The initial Coulombic efficiency of L12 was 77.4%, whereas that of L15 was 74.1%. Also, L12 and L15 exhibited similar voltage profiles by comparison of the 1st discharge, 3rd discharge, and 31st discharge, as shown in Figure 7b.



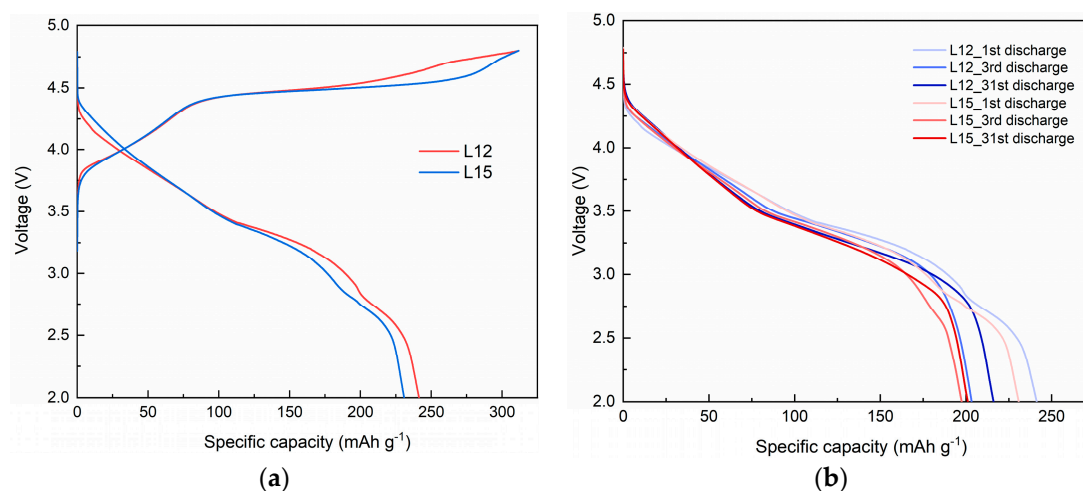


**Figure 7.** (a) Initial charge–discharge profiles of L12 and L15 at 0.03C within 2.0–4.8 V; (b) Voltage profiles of L12 and L15 for comparison of the 1st discharge, 3rd discharge and 31st discharge.

**Table 6.** Initial charge–discharge performance of L12 and L15 at 0.03 C in the range of 2.0–4.8 V.

Sample	Lithium Source	Initial Charge Capacity/mAh g <sup>-1</sup>	Initial Discharge Capacity/mAh g <sup>-1</sup>	Irreversible Capacity/mAh g <sup>-1</sup>	Initial Coulombic Efficiency/%
L12	Li <sub>2</sub> CO <sub>3</sub>	311.75	241.34	70.41	77.4
L15	LiOH	311.66	230.86	80.80	74.1

Figure 8a shows the cycling performance of L12 and L15 in the range of 2.0–4.8 V. These samples had a similar capacity loss for charge–discharge curves in the first and second cycles. This process may be related to oxygen release during Li<sub>2</sub>MnO<sub>3</sub> activation in the first cycle and may lead to structural rearrangement at 0.1 C during the second cycle [8,39]. The charge–discharge curves of L12 and L15 gradually became stable with increasing cycle numbers. However, L12 exhibited a more stable cycling performance and a higher capacity retention after 30 cycles. L12 maintained a discharge capacity of 216 mAh g<sup>-1</sup> and a capacity retention of 89.6%, whereas L15 had a discharge capacity of 201.2 mAh g<sup>-1</sup> and a capacity retention of 87.1%. In addition, the cycling performance of L12 and that of L15 were compared in the two ranges of 2.0–4.8 V and 2.0–4.6 V, as Figure 8b shows. In the range between 2.0 and 4.6 V, L12 and L15 delivered lower initial charge/discharge capacities of 240.31/176.63 mAh g<sup>-1</sup> and 277.96/223.99 mAh g<sup>-1</sup>, respectively. After the first cycle, the discharge capacity of both samples, but especially of L12, gradually increased with increasing cycle numbers. This revealed that a range of 2.0–4.6 V could not entirely activate Li<sub>2</sub>MnO<sub>3</sub> during the first cycle. The continuous activation of the Li<sub>2</sub>MnO<sub>3</sub> component increased discharge capacity in the subsequent cycles. However, the discharge capacity of L12 and L15 after 30 cycles in the range of 2.0–4.6 V was still lower than that in the range of 2.0–4.8 V. Therefore, an optimized range of 2.0–4.8 V was used to effectively activate the Li<sub>2</sub>MnO<sub>3</sub> component and improve cycling stability in the subsequent studies. L12 exhibited a higher capacity retention than L15 in both the 2.0–4.8 V and 2.0–4.6 V ranges. These results suggested that the material prepared using Li<sub>2</sub>CO<sub>3</sub> as a lithium source exhibited better electrochemical performance.

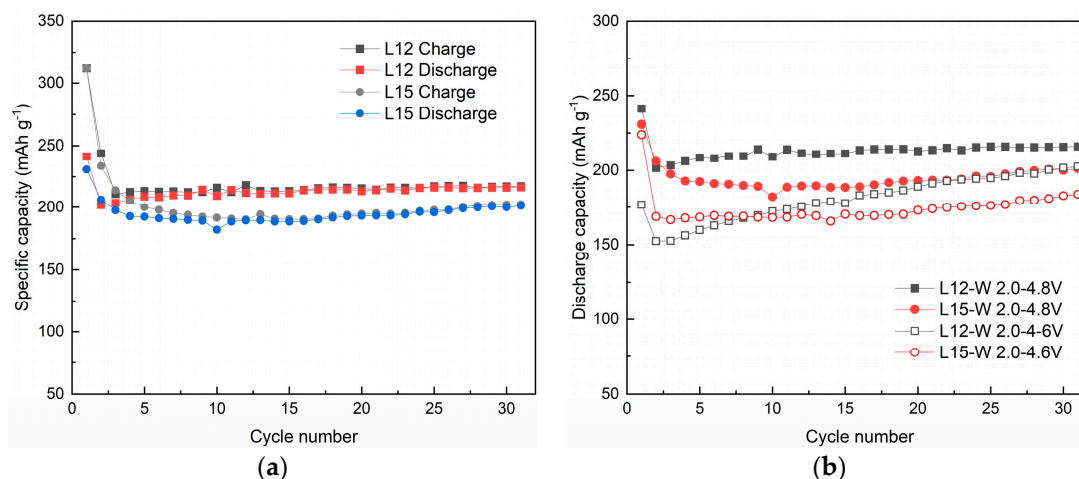


**Figure 8.** (a) Charge–discharge curves of L12 and L15 for 30 cycles within 2.0–4.8 V; (b) Cycling performance of L12 and that of L15 were compared in 2.0–4.8 V and 2.0–4.6 V for 30 cycles.

#### 4. Conclusions

The precursors of lithium-rich manganese-based cathode materials were prepared using hydroxide coprecipitation. A two-step calcination process was used to synthesize LLO cathode materials. The first stage consisted of preheating at 500 °C for 5 h to ensure a homogenous lithiation of precursors and lithium sources. The second step consisted of calcination at 850 °C for 12 h, which completed the lithiation reaction. The XRD results confirmed that the selected calcination temperature and time enabled the synthesis of well-layered materials and ensured that the materials had no impurities. The crystal structure of the prepared LLO cathode materials exhibited certain defects or stacking faults. Furthermore, the material prepared using the lithium source Li<sub>2</sub>CO<sub>3</sub> and that prepared using LiOH had similar structural properties. The material associated with Li<sub>2</sub>CO<sub>3</sub> exhibited better electrochemical performance than that associated with LiOH. Lithium content had a significant impact on the structure and electrochemical performance of LLO cathode materials. In this study, L10 had a good crystalline structure and delivered the best electrochemical performance. L10 reached the highest initial discharge capacity (279.65 mAh g<sup>-1</sup>) and initial Coulombic efficiency (82.8%) at 0.03 C. It delivered a discharge capacity of 231.9 mAh g<sup>-1</sup> and a capacity retention of 82.9% at 0.1 C after 30 cycles. All samples had an irreversible capacity loss of approximately 20% in the first cycle and could reach a discharge capacity of over 200 mAh g<sup>-1</sup> after 30 cycles.

In summary, the synthesized LLO cathode materials had some drawbacks, including undesired morphology, low tap density, irreversible capacity loss in the first cycle, and voltage fading during cycling. To improve electrochemical performance, further work on the optimization of synthesis conditions in coprecipitation and chemical composition is necessary. Research needs to provide advanced characterization techniques for in-depth understanding of the relationship of synthesis conditions/composition/structure/electrochemical behaviors. Moreover, research work focused on improvement of LLO cathode materials to accelerate industrialization, but also giving consideration to both cost-effectiveness and environmental compatibility, is significant.

**Author Contributions:** Conceptualization, Y.W., M.H. and P.T.; methodology, Y.W., M.H., J.V. and T.H.; investigation, Y.W., M.H., J.V., T.H. and P.T.; writing—original draft preparation, Y.W. and M.H.; writing—review and editing, J.V., T.H., P.T. and U.L.; visualization, Y.W. and J.V.; supervision, U.L. and P.T.; project administration, U.L.; funding acquisition, U.L. All authors have read and agreed to the published version of the manuscript.

**Funding:** This research was funded by Business Finland for research funding in 2021–2024 (University of Oulu, BATCircle2.0, Dnro 44612/31/2020).

**Data Availability Statement:** Not applicable.

**Conflicts of Interest:** The authors declare no conflict of interest.

## References

1. Zuo, W.; Luo, M.; Liu, X.; Wu, J.; Liu, H.; Li, J.; Winter, M.; Fu, R.; Yang, W.; Yang, Y. Li-rich cathodes for rechargeable Li-based batteries: Reaction mechanisms and advanced characterization techniques. *Energy Environ. Sci.* **2020**, *13*, 4450–4497. [\[CrossRef\]](#)
2. Li, W.; Song, B.; Manthiram, A. High-voltage positive electrode materials for lithium-ion batteries. *Chem. Soc. Rev.* **2017**, *46*, 3006–3059. [\[CrossRef\]](#)
3. Yan, J.; Liu, X.; Li, B. Recent progress in Li-rich layered oxides as cathode materials for Li-ion batteries. *RSC Adv.* **2014**, *4*, 63268–63284. [\[CrossRef\]](#)
4. Yu, H.; Zhou, H. High-Energy Cathode Materials ( $\text{Li}_2\text{MnO}_3\text{-LiMO}_2$ ) for Lithium-Ion Batteries. *J. Phys. Chem. Lett.* **2013**, *4*, 1268–1280. [\[CrossRef\]](#)
5. Manthiram, A.; Knight, J.C.; Myung, S.-T.; Oh, S.-M.; Sun, Y.-K. Nickel-Rich and Lithium-Rich Layered Oxide Cathodes: Progress and Perspectives. *Adv. Energy Mater.* **2016**, *6*, 1501010. [\[CrossRef\]](#)
6. Zheng, J.; Myeong, S.; Cho, W.; Yan, P.; Xiao, J.; Wang, C.; Cho, J.; Zhang, J.G. Li- and Mn-Rich Cathode Materials: Challenges to Commercialization. *Adv. Energy Mater.* **2016**, *7*, 1601284. [\[CrossRef\]](#)
7. Lei, Y.; Ni, J.; Hu, Z.; Wang, Z.; Gui, F.; Li, B.; Ming, P.; Zhang, C.; Elias, Y.; Aurbach, D.; et al. Surface Modification of Li-Rich Mn-Based Layered Oxide Cathodes: Challenges, Materials, Methods, and Characterization. *Adv. Energy Mater.* **2020**, *10*, 2002506. [\[CrossRef\]](#)
8. Thackeray, M.M.; Johnson, C.S.; Vaughey, J.T.; Li, N.; Hackney, S.A. Advances in manganese-oxide ‘composite’ electrodes for lithium-ion batteries. *J. Mater. Chem.* **2005**, *15*, 2257–2267. [\[CrossRef\]](#)
9. Hy, S.; Liu, H.; Zhang, M.; Qian, D.; Hwang, B.-J.; Meng, Y.S. Performance and design considerations for lithium excess layered oxide positive electrode materials for lithium ion batteries. *Energy Environ. Sci.* **2016**, *9*, 1931–1954. [\[CrossRef\]](#)
10. Pan, H.; Zhang, S.; Chen, J.; Gao, M.; Liu, Y.; Zhu, T.; Jiang, Y. Li- and Mn-rich layered oxide cathode materials for lithium-ion batteries: A review from fundamentals to research progress and applications. *Mol. Syst. Des. Eng.* **2018**, *3*, 748–803. [\[CrossRef\]](#)
11. He, W.; Guo, W.; Wu, H.; Lin, L.; Liu, Q.; Han, X.; Xie, Q.; Liu, P.; Zheng, H.; Wang, L.; et al. Challenges and Recent Advances in High Capacity Li-Rich Cathode Materials for High Energy Density Lithium-Ion Batteries. *Adv. Mater.* **2021**, *33*, e2005937. [\[CrossRef\]](#)
12. Rossouw, M.H.; Thackeray, M.M. Lithium manganese oxides from  $\text{Li}_2\text{MnO}_3$  for rechargeable lithium battery applications. *Mater. Res. Bull.* **1991**, *26*, 463–473. [\[CrossRef\]](#)
13. Numata, K.; Sakaki, C.; Yamanaka, S. Synthesis of Solid Solutions in a System of  $\text{LiCoO}_2\text{-Li}_2\text{MnO}_3$  for Cathode Materials of Secondary Lithium Batteries. *Chem. Lett.* **1997**, *26*, 725–726. [\[CrossRef\]](#)
14. Numata, K.; Sakaki, C.; Yamanaka, S. Synthesis and characterization of layer structured solid solutions in the system of  $\text{LiCoO}_2\text{-Li}_2\text{MnO}_3$ . *Solid State Ion.* **1999**, *117*, 257–263. [\[CrossRef\]](#)
15. Kalyani, P.; Chitra, S.; Mohan, T.; Gopukumar, S. Lithium metal rechargeable cells using  $\text{Li}_2\text{MnO}_3$  as the positive electrode. *J. Power Sources* **1999**, *80*, 103–106. [\[CrossRef\]](#)
16. Lu, Z.; MacNeil, D.D.; Dahn, J.R. Layered Cathode Materials  $\text{Li}[\text{Ni}_x\text{Li}_{(1/3-2x/3)}\text{Mn}_{(2/3-x/3)}]\text{O}_2$  for Lithium-Ion Batteries. *Electrochem. Solid-State Lett.* **2001**, *4*, A191. [\[CrossRef\]](#)
17. Lu, Z.; Dahn, J.R. Structure and Electrochemistry of Layered  $\text{Li}[\text{Cr}_x\text{Li}_{(1/3-x/3)}\text{Mn}_{(2/3-2x/3)}]\text{O}_2$ . *J. Electrochem. Soc.* **2002**, *149*, A1454. [\[CrossRef\]](#)
18. Kim, J.-S.; Johnson, C.S.; Vaughey, J.T.; Thackeray, M.M.; Hackney, S.A.; Yoon, W.; Grey, C.P. Electrochemical and Structural Properties of  $x\text{Li}_2\text{M}'\text{O}_3 \cdot (1-x)\text{LiMn}_{0.5}\text{Ni}_{0.5}\text{O}_2$  Electrodes for Lithium Batteries ( $\text{M}' = \text{Ti, Mn, Zr}$ ;  $0 \leq x \leq 0.3$ ). *Chem. Mater.* **2004**, *16*, 1996–2006. [\[CrossRef\]](#)
19. Jarvis, K.A.; Deng, Z.; Allard, L.F.; Manthiram, A.; Ferreira, P.J. Atomic Structure of a Lithium-Rich Layered Oxide Material for Lithium-Ion Batteries: Evidence of a Solid Solution. *Chem. Mater.* **2011**, *23*, 3614–3621. [\[CrossRef\]](#)
20. Koga, H.; Croguennec, L.; Mannesiez, P.; Ménétrier, M.; Weill, F.; Bourgeois, L.; Duttine, M.; Suard, E.; Delmas, C.  $\text{Li}_{1.20}\text{Mn}_{0.54}\text{Co}_{0.13}\text{Ni}_{0.13}\text{O}_2$  with Different Particle Sizes as Attractive Positive Electrode Materials for Lithium-Ion Batteries: Insights into Their Structure. *J. Phys. Chem. C* **2012**, *116*, 13497–13506. [\[CrossRef\]](#)
21. Shukla, A.K.; Ramasse, Q.M.; Ophus, C.; Duncan, H.; Hage, F.; Chen, G. Unravelling structural ambiguities in lithium- and manganese-rich transition metal oxides. *Nat. Commun.* **2015**, *6*, 8711. [\[CrossRef\]](#)
22. Song, Y.; Zhao, X.; Wang, C.; Bi, H.; Zhang, J.; Li, S.; Wang, M.; Che, R. Insight into the atomic structure of  $\text{Li}_2\text{MnO}_3$  in Li-rich Mn-based cathode materials and the impact of its atomic arrangement on electrochemical performance. *J. Mater. Chem. A* **2017**, *5*, 11214–11223. [\[CrossRef\]](#)
23. Yabuuchi, N.; Yoshii, K.; Myung, S.T.; Nakai, I.; Komaba, S. Detailed studies of a high-capacity electrode material for rechargeable batteries,  $\text{Li}_2\text{MnO}_3\text{-LiCo}_{(1/3)}\text{Ni}_{(1/3)}\text{Mn}_{(1/3)}\text{O}_2$ . *J. Am. Chem. Soc.* **2011**, *133*, 4404–4419. [\[CrossRef\]](#)
24. Johnson, C.S.; Kim, J.S.; Lefief, C.; Li, N.; Vaughey, J.T.; Thackeray, M.M. The significance of the  $\text{Li}_2\text{MnO}_3$  component in ‘composite’  $x\text{Li}_2\text{MnO}_3 \cdot (1-x)\text{LiMn}_{0.5}\text{Ni}_{0.5}\text{O}_2$  electrodes. *Electrochem. Commun.* **2004**, *6*, 1085–1091. [\[CrossRef\]](#)

25. Johnson, C.S.; Li, N.; Lefief, C.; Thackeray, M.M. Anomalous capacity and cycling stability of  $x\text{Li}_2\text{MnO}_3 \cdot (1-x)\text{LiMO}_2$  electrodes (M=Mn, Ni, Co) in lithium batteries at 50 °C. *Electrochem. Commun.* **2007**, *9*, 787–795. [[CrossRef](#)]
26. Thackeray, M.M.; Kang, S.-H.; Johnson, C.S.; Vaughey, J.T.; Benedek, R.; Hackney, S.A.  $\text{Li}_2\text{MnO}_3$ -stabilized  $\text{LiMO}_2$  (M = Mn, Ni, Co) electrodes for lithium-ion batteries. *J. Mater. Chem.* **2007**, *17*, 3112–3125. [[CrossRef](#)]
27. Zheng, J.; Gu, M.; Genc, A.; Xiao, J.; Xu, P.; Chen, X.; Zhu, Z.; Zhao, W.; Pullan, L.; Wang, C.; et al. Mitigating voltage fade in cathode materials by improving the atomic level uniformity of elemental distribution. *Nano Lett.* **2014**, *14*, 2628–2635. [[CrossRef](#)]
28. Fu, F.; Yao, Y.; Wang, H.; Xu, G.L.; Amine, K.; Sun, S.; Shao, M. Structure dependent electrochemical performance of Li-rich layered oxides in lithium-ion batteries. *Nano Energy* **2017**, *35*, 370–378. [[CrossRef](#)]
29. Pimenta, V.; Sathiya, M.; Batuk, D.; Abakumov, A.M.; Giaume, D.; Cassaignon, S.; Larcher, D.; Tarascon, J.-M. Synthesis of Li-Rich NMC: A Comprehensive Study. *Chem. Mater.* **2017**, *29*, 9923–9936. [[CrossRef](#)]
30. Cao, K.; Shen, T.; Wang, K.; Chen, D.; Wang, W. Influence of different lithium sources on the morphology, structure and electrochemical performances of lithium-rich layered oxides. *Ceram. Int.* **2017**, *43*, 8694–8702. [[CrossRef](#)]
31. Gao, S.; Zhang, Y.; Zhang, H.; Song, D.; Shi, X.; Zhang, L. The effect of lithium content on the structure, morphology and electrochemical performance of Li-rich cathode materials  $\text{Li}_{1+x}(\text{Ni}_{1/6}\text{Co}_{1/6}\text{Mn}_{4/6})_{1-x}\text{O}_2$ . *New J. Chem.* **2017**, *41*, 10048–10053. [[CrossRef](#)]
32. Yang, X.; Wang, X.; Wei, Q.; Shu, H.; Liu, L.; Yang, S.; Hu, B.; Song, Y.; Zou, G.; Hu, L.; et al. Synthesis and characterization of a Li-rich layered cathode material  $\text{Li}_{1.15}[(\text{Mn}_{1/3}\text{Ni}_{1/3}\text{Co}_{1/3})_{0.5}(\text{Ni}_{1/4}\text{Mn}_{3/4})_{0.5}]_{0.85}\text{O}_2$  with spherical core-shell structure. *J. Mater. Chem.* **2012**, *22*, 19666–19672. [[CrossRef](#)]
33. Meng, Y.S.; Ceder, G.; Grey, C.P.; Yoon, W.S.; Jiang, M.; Bréger, J.; Shao-Horn, Y. Cation Ordering in Layered  $\text{O}_3$   $\text{Li}[\text{Ni}_x\text{Li}_{1/3-2x/3}\text{Mn}_{2/3-x/3}]\text{O}_2$  ( $0 \leq x \leq 1/2$ ) Compounds. *Chem. Mater.* **2005**, *17*, 2386–2394. [[CrossRef](#)]
34. Boulineau, A.; Croguennec, L.; Delmas, C.; Weill, F. Structure of  $\text{Li}_2\text{MnO}_3$  with different degrees of defects. *Solid State Ion.* **2010**, *180*, 1652–1659. [[CrossRef](#)]
35. Shunmugasundaram, R.; Arumugam, R.S.; Dahn, J.R. A Study of Stacking Faults and Superlattice Ordering in Some Li-Rich Layered Transition Metal Oxide Positive Electrode Materials. *J. Electrochem. Soc.* **2016**, *163*, A1394–A1400. [[CrossRef](#)]
36. Wang, M.-J.; Shao, A.-F.; Yu, F.-D.; Sun, G.; Gu, D.-M.; Wang, Z.-B. Simple Water Treatment Strategy To Optimize the  $\text{Li}_2\text{MnO}_3$  Activation of Lithium-Rich Cathode Materials. *ACS Sustain. Chem. Eng.* **2019**, *7*, 12825–12837. [[CrossRef](#)]
37. Xiang, Y.; Yin, Z.; Zhang, Y.; Li, X. Effects of synthesis conditions on the structural and electrochemical properties of the Li-rich material  $\text{Li}[\text{Li}_{0.2}\text{Ni}_{0.17}\text{Co}_{0.16}\text{Mn}_{0.47}]\text{O}_2$  via the solid-state method. *Electrochim. Acta* **2013**, *91*, 214–218. [[CrossRef](#)]
38. Shunmugasundaram, R.; Senthil Arumugam, R.; Dahn, J.R. High Capacity Li-Rich Positive Electrode Materials with Reduced First-Cycle Irreversible Capacity Loss. *Chem. Mater.* **2015**, *27*, 757–767. [[CrossRef](#)]
39. Wenfeng, R.; Zhao, Y.; Hu, X.; Xia, M. Preparation-microstructure-performance relationship of Li-rich transition metal oxides microspheres as cathode materials for lithium ion batteries. *Electrochim. Acta* **2016**, *191*, 491–499. [[CrossRef](#)]

**Disclaimer/Publisher’s Note:** The statements, opinions and data contained in all publications are solely those of the individual author(s) and contributor(s) and not of MDPI and/or the editor(s). MDPI and/or the editor(s) disclaim responsibility for any injury to people or property resulting from any ideas, methods, instructions or products referred to in the content.